IEEE Journal of Microwaves

Received 25 April 2023; revised 26 May 2023 and 28 June 2023; accepted 12 July 2023. Date of publication 3 August 2023; date of current version 9 October 2023.

Digital Object Identifier 10.1109/JMW.2023.3296594

A Simple and Versatile Concept to Improve Dynamic Range and Enable Target Angle Adaptability in Radar Target Simulators

CHRISTOPH BIRKENHAUER [1] (Graduate Student Member, IEEE), GEORG KÖRNER [1], PATRICK STIEF [1], GERHARD HAMBERGER [2], MATTHIAS BEER [2], CHRISTIAN CARLOWITZ [1] (Member, IEEE), AND MARTIN VOSSIEK [1] (Fellow, IEEE)

(Regular Paper)

[1]Institute of Microwaves and Photonics, Friedrich-Alexander-Universität Erlangen-Nürnberg, 91054 Erlangen, Germany
[2]Rohde & Schwarz GmbH & Co. KG, 81671 Munich, Germany

CORRESPONDING AUTHOR: Christoph Birkenhauer (e-mail: christoph.birkenhauer@fau.de).

This work was supported by the Bavarian Ministry of Economic Affairs, Regional Development and Energy as part of the program "Informations- und Kommunikationstechnik ELSYS" under Grant ESB-1809–0007.

ABSTRACT Radar target simulators are not only a critical tool for verifying and testing radar systems but also play an important role in supporting the development of self-driving cars. Advances in radar sensors and techniques raise the required specifications for these units, increasing their complexity and cost. This article presents a novel and universal concept for radar target simulators that addresses these issues by responding only to the transmitted signal of a radar sensor during a fraction of the time, therefore modulating the average of the signal. This offers advantages for three independent use cases, which may be combined. First, the dynamic range and resolution of simulated target echo power can be improved even for existing systems. Second, the simulation of multiangle scenarios with a single backend is possible with this approach. Finally, hardware complexity and power consumption can be reduced. The proposed concept is examined extensively for frequency-modulated continuous wave radar, and design decisions are made. The theoretical considerations are validated with measurements with a real radar target simulator showing an improvement of up to 30 dB in the dynamic range with no observable negative side effects.

INDEX TERMS Automotive radar, radar target simulator, TDM, radar signal processing, radar systems.

I. INTRODUCTION

Radar target simulators (RTSs) are used to emulate well-defined targets or scenarios to test radar sensors or the behavior of entire systems that include such sensors [1], [2], [3]. This makes it possible to test vehicles in a vehicle-in-the-loop setup, including the simulation of their environment [4], [5]. The environment can be described as a composition of point targets created by an antenna array similar to the pixels of a digital screen, as shown in Fig. 1. However, each target can convey more information than just its reflectance. Distance and motion are represented by a time-dependent delay τ_T of the signal, which can be introduced by shifting stored samples in the digital domain [6] or by using a delay line [7] in combination with a mixing process to introduce a Doppler shift [8]. A generalized implementation of an RTS with an additional frequency conversion is depicted in Fig. 2. For the sake of completeness, an additional approach exists for frequency-modulated continuous wave (FMCW) and frequency-stepped continuous wave (FSCW) radar; here the signal can be manipulated by modulation so that the resulting baseband signal appears to carry the attributes of the desired target without matching the physical behavior of a real target [9]. Knowledge of the ramp slope is required through either prior information [10] or the analysis of multiple ramps [11] for the modulation. These implementations differ substantially, and all are limited in terms of their

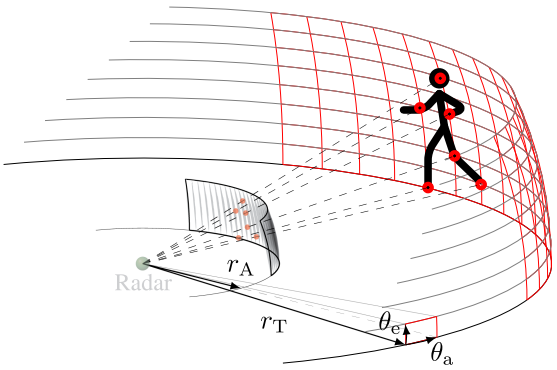

FIGURE 1. An illustrative example of a simulated scene created by an radar target simulator (RTS). The scene appears in the area behind the physical location of the antenna array, which is placed in front of the sensor. A closely populated antenna array is required for precise angular representation.

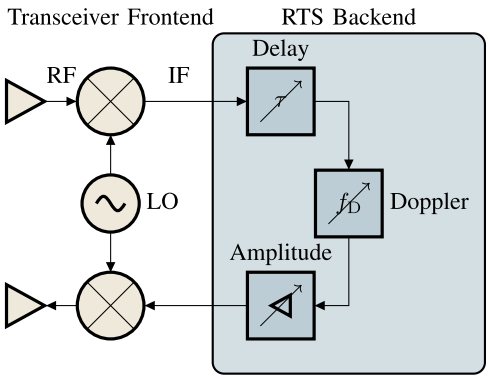

FIGURE 2. Typical radar target simulator consisting of a bistatic antenna setup and a transceiver unit for frequency conversion. The actual alteration of the signal is done by the backend.

scalability. While a single target may be represented by a moving antenna [12], complex scenarios require a multitude of simultaneous point targets and therefore, multiple backends [13], which increases the costs. For arbitrary angle-of-arrival simulations, the spacing of the individual elements must be lower than the angular resolution of the radar [14]. With recent advances in integrated radar sensors [15] and techniques, such as coherent automotive radar networks [16], the requirements for the minimal vertical and horizontal angular resolution θ_e and θ_a between different point targets have increased. This is especially problematic for digital RTSs, as they are the most expensive due to the requirement for special analog-to-digital converters (ADCs) and digital-to-analog converters (DACs) with high sample rates and low latency [6]. Another shared problem is the relatively small achievable dynamic range compared to the huge dynamic range required for the depiction of a variety of regular targets [17]. Therefore, the challenges for future RTSs that enable complex scenarios are mainly cost and hardware complexity, as well as dynamic range considerations. We will show that these challenges can be addressed by responding to the radar for only a fraction of the time. This frees up resources to emulate

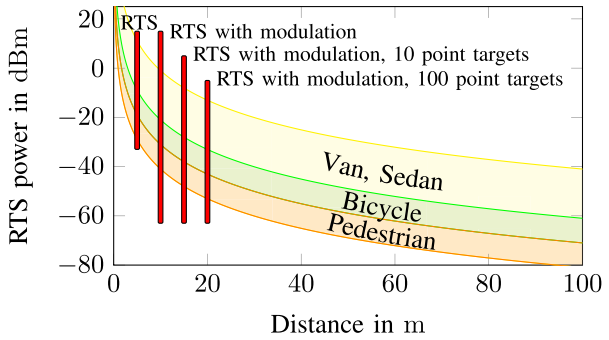

FIGURE 3. The transmit power required for different scenarios is shown. The red bars depict dynamic ranges that can be created with different utilizations of the modulation scheme. The modulation can be used to improve the dynamic range or increase the number of simulated channels.

multiple target angles during different time frames with a single backend channel. If done correctly, the radar under test (RUT) perceives multiple targets created by a single backend channel at the same time. Clearly, this has enormous potential for cost savings and improvement in spatial resolution; however, the dynamic range can also be improved with a timing scheme similar to pulse width modulation (PWM). Multiple target responses can be attenuated with this method before being combined and sent to the radar. Naturally, this is not possible with attenuators or adjustable amplifiers. Finally, providing a radar echo for only a fraction of the time has other practical advantages, as this can be used to decrease the required storage and processing capabilities or reduce the power consumption by turning the complete backend off for some time [18]. The power that a radar sensor receives from an RTS needs to match that of a real target. The required transmit power of the RTS can be calculated by equating the radar equation [19, p. 4] with the power received from a transmitter [20]. After solving for the transmit power $P_{TX,RTS}$ of the RTS, the relation

$$P_{TX,RTS} = P_{TX,R} \cdot \frac{G_R \cdot {r_A}^2 \cdot \sigma^2}{G_{RTS} \cdot {r_T}^4 \cdot 4\pi} \tag{1}$$

can be derived for an RTS that is placed at the distance r_A in front of the radar while simulating a target at the distance r_T. The transmit power $P_{TX,R}$ and the antenna gain G_R of the radar must to be considered, as well as the gain of the RTS antenna G_{RTS}. By inserting the radar cross section (RCS) σ of three different road users given in [21] in (1), the required transmit power $P_{TX,RTS}$ of the RTS can be plotted for an illustrative system, as visualized in Fig. 3, which is positioned at the distance $r_A = 1\,\text{m}$ in front of the radar. A maximum transmit power of 15 dBm is assumed for the system, while all antenna gains are set to 10 dBi. As can be seen from the plots, a high dynamic range of the RTS transmit power is required if different road users, such as pedestrians and vans, are simulated simultaneously. For scenarios with differing distances, the required dynamic range only increases. In contrast, the dynamic range for the standard RTS is assumed to be 48 dB, the maximum theoretical achievable value for an

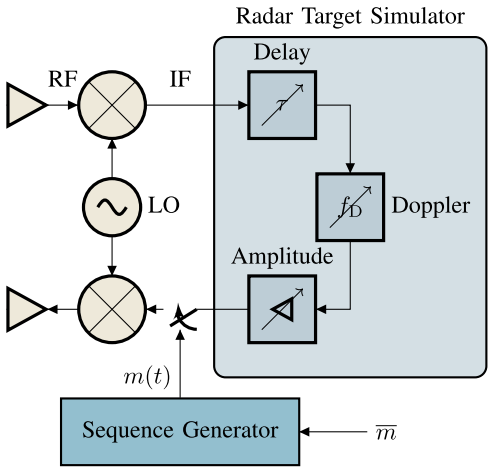

FIGURE 4. Preexisting target simulator with an added switch and an sequence generator. The goal of the sequence generator is to create a modulation that limits the creation of unwanted ghost targets.

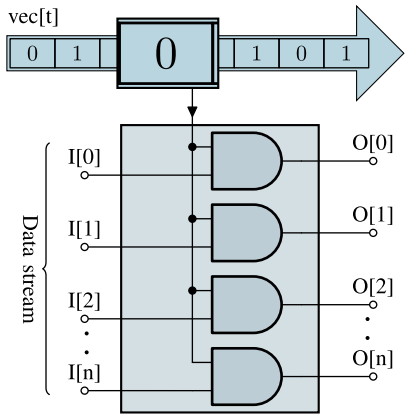

FIGURE 5. Implementation of the modulation scheme within a digital RTS, which is also used for the demonstrator. The data stream is controlled by AND gates, which are driven by a predefined pseudo-random sequence.

8-bit system, which is not unusual for a digital RTS. This range is depicted by the first red bar in Fig. 3. With the modulation, an increase of 30 dB for the dynamic range of the RTS is assumed, as the average output power can be decreased below the minimum output power of the unmodulated system. With this, the combined dynamic range depicted by the second bar can be achieved. Alternatively, the modulation can be used to enable multiangle scenarios by switching a single RTS between multiple antennas. This naturally reduces the transmitted power for each antenna, resulting in reduced maximum average output power. The resulting dynamic range for this setup is depicted by the last two bars for 10 and 100 point targets with different angles. By comparing the resulting dynamic range of the modulated RTS with the classical approach, improvements in the concept can be observed. The achievable distance ranges for complex scenarios with plausible RCS values allow for the creation of more realistic scenes. Additionally, multiangle scenarios become possible in a cost-effective manner with modulation, as only one RTS backend is required. This work focuses on FMCW radars, which are the dominant radar technology today. While the underlying principles considered apply to other sensors, our approach benefits from the relatively small bandwidth of FMCW radar sensors as discussed later.

II. PROPOSED SYSTEM SETUP

To increase the dynamic range for a single target, any preexisting RTS may be used in combination with a simple switch in the return path, as shown in Fig. 4. The change in signal strength, and therefore, the apparent RCS, can be described with the linear scaling factor $\overline{m}$. A sequence generator is added to convert $\overline{m}$ to a modulation sequence, which is then applied to the switch. The main function of this generator is to produce a modulation $m(t)$, which results in small magnitudes of spurious components for at least short observation intervals. This reduces the appearance of unwanted ghost targets. Predefined pseudo-random sequences or dynamic changes in the modulation frequency may be used to achieve this. As most state-of-the-art RTSs use digital backends based on programmable logic, modulation can be applied before the signal is put into the analog domain with a DAC. Instead of a switch, logical gates can be used to disable the data stream, as shown in Fig. 5. As another advantage compared to an analog switch, multiple data streams can be recombined for highly dynamic scenarios, where multiple targets at different distances need different switching processes. The desired attenuation can be created by iterating through a predefined sequence of binary values, where their mean equals $\overline{m}$. Consequently, the data stream may be calculated only for the periods in which the samples are applied instead. This increases the overall efficiency and allows for low-cost and low-power implementations. Another possibility created by the intermittent provision of a radar response is to free up a capable backend for other operations, such as alternating between calculations for multiple channels. An RTS based on this principle is illustrated in Fig. 6. In the figure, an antenna array is used to alternate between multiple receive and transmit paths. A single RTS backend is then used to generate the signal manipulation for all channels in a time division multiplexing (TDM) scheme. Synchronization for both changing the antenna configuration and the parameters of the RTS ensures that a valid response for each channel is produced during a sufficient amount of time. This implementation might hold the greatest benefits for upcoming highly capable target simulators. Complicated and realistic scenes, including a multitude of point targets with varying angles, could be created by the combination of a capable antenna array and one digital backend channel. The cost benefit associated with this might hold the key to commercially feasible target simulators that are able to create three-dimensional scenes with good resolution, as depicted in Fig. 1.

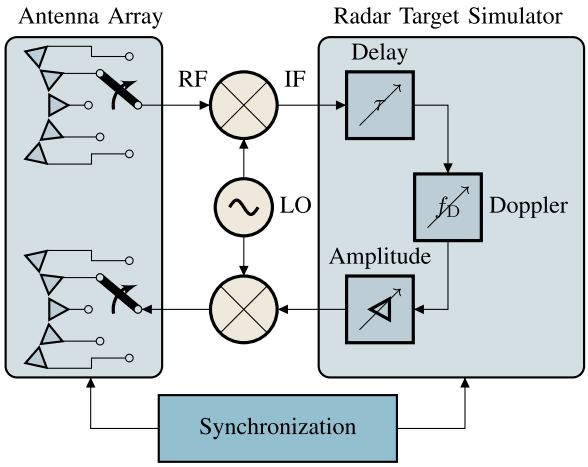

FIGURE 6. RTS with a multiangle antenna array, where a single backend is switched between several channels to create complex scenarios. If the switching is fast enough, multiple targets with different angles can be represented simultaneously.

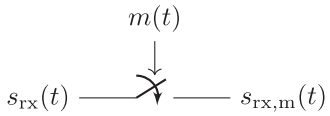

FIGURE 7. Switching process of the input signal $s_{\mathrm{rx}}(t)$ by the modulation function $m(t)$. An ideal switch is assumed for the following considerations.

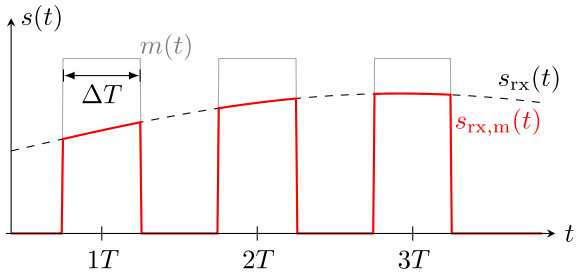

FIGURE 8. Modulated signal $s_{\mathrm{rx,m}}(t)$ in the time domain in red with periodic modulation and the unmodulated base signal $s_{\mathrm{rx}}(t)$ in the background. An ideal switch alternating between the states "on" and "off" is assumed.

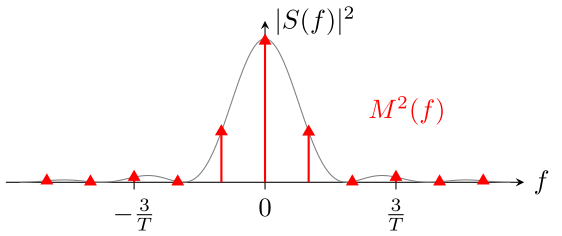

FIGURE 9. Frequency domain representation of the signal distribution introduced by the periodic modulation. The original spectrum $S_{\mathrm{rx}}(f)$ is repeated and centered at each i/T-th frequency while the absolute value depends on $\Delta T/T$ in combination with the si-function.

III. SIGNAL MODEL AND OPERATING PRINCIPLE

The perceived signal strength of the signal received will decrease with the application of the modulation. However, additional effects and their impact on radar sensors also need to be investigated. The signal $s_{\mathrm{rx}}(t)$ is considered received by the radar unit with the transmitted signal $s_{\mathrm{tx}}(t)$. The RTS provides a delay that represents the difference in the simulated distance r_{T} and the physical distance between the radar and RTS. To describe the distance and movement, a time-dependent delay τ_{T} is assumed. Neglecting the amplitude, the signal a radar receives can be represented as

$$s_{\mathrm{rx}}(t) = s_{\mathrm{tx}}(t - \tau_{\mathrm{T}}(t)) \,. \tag{2}$$

To allow for a simple and efficient implementation, a switching process between the states "on" and "off" is considered without any transition duration between these states, similar to a rectangular window function, as shown in Fig. 7. The modulated signal $s_{\mathrm{rx,m}}(t)$ received by the radar can therefore be described by

$$s_{\mathrm{rx,m}}(t) = s_{\mathrm{tx}}(t - \tau_{\mathrm{T}}(t)) \cdot m(t) = s_{\mathrm{rx}}(t) \cdot m(t) \tag{3}$$

with the modulation function $m(t)$. It is sufficient to consider $s_{\mathrm{rx}}(t)$ as a signal that would result in an ideal target after signal processing, maintaining attention on the additional modulation. Assuming for now that $m(t)$ is periodic at each on-off stage, it can be described by

$$m(t) = \sum_{n=-\infty}^{\infty} \mathrm{rect}\left(\frac{t - nT}{\Delta T}\right) , \tag{4}$$

where ΔT represents the duration for which the signal is enabled and T the period time achievable by the switching process. The resulting time domain signal for (3) is illustrated in Fig. 8. Equations (3) and (4) can be combined and rewritten into (5):

$$s_{\mathrm{rx,m}}(t) = s_{\mathrm{rx}}(t) \left[\mathrm{rect}\left(\frac{t}{\Delta T}\right) * \sum_{n=-\infty}^{\infty} \delta(t - nT) \right] , \tag{5}$$

$$\Downarrow$$

$$S_{\mathrm{rx,m}}(f) = S_{\mathrm{rx}}(f) * \underbrace{\left[\frac{\Delta T}{T} \, \mathrm{si}(\pi f \Delta T) \sum_{i=-\infty}^{\infty} \delta\left(f - \frac{i}{T}\right) \right]}_{M(f)} . \tag{6}$$

Equation (6) is obtained by converting (5) into the frequency domain. It can be clearly observed by evaluating (6) that the switching process creates a multitude of additional components within the spectrum when compared to $S_{\mathrm{rx}}(f)$. The undesired components of the power spectrum $M^2(f)$ are spread over a wide range in the frequency domain, as depicted in Fig. 9, while the main component is scaled by the factor $(\frac{\Delta T}{T})^2$. Therefore, providing a valid response for only a fraction of the radar signal duration will result in the creation of unwanted spectral components. This is undesirable, as these components may then be interpreted as false targets by the radar if no mitigation is implemented. From (6), we

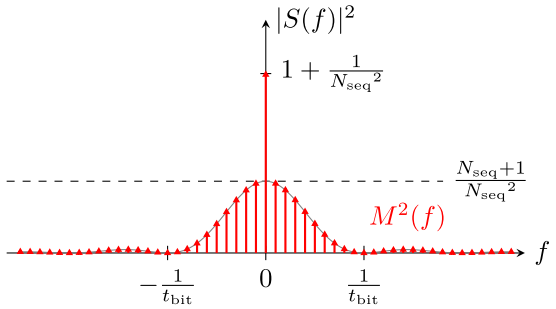

FIGURE 10. Normalized representation of the spectral components for the modulation considered based on a pseudo-random binary sequence. The magnitudes of the unwanted spectral components are reduced with the increasing sequence length, while the constant component is almost unaffected.

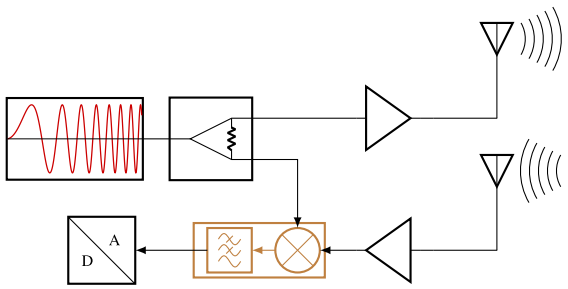

FIGURE 11. Block diagram of an FMCW radar sensor. The frequency of the signal changes linearly over time. Due to the distance between the radar sensor and the target, the signal reflected is perceived at a different frequency. The difference is examined by mixing the two signals. The signal difference is then in a linear relation to the target distance.

can determine the ratio between the first spurious component in comparison to the main signal with

$$\frac{S^2(f_1)}{S^2(f_0)} = \frac{M^2_{i=1}(\frac{1}{T})}{M^2_{i=0}(0)} = \mathrm{si}^2\left(\pi\frac{\Delta T}{T}\right), \tag{7}$$

which can be used to assess the spurious-free dynamic range (SFDR) of the output signal, as the first spur is also the largest. Therefore, for a duty cycle of 50%, the first spurious component is of high value ($S(f_1) \approx 0.41 \cdot S(f_0)$), resulting in an SFDR of only 3.87 dB. This represents the worst-case consideration if no additional processing steps are taken. To improve the SFDR, the spectral components can be spread over a wider range by randomization of the modulation scheme [22] during the observation time of the radar. A pseudo-random binary sequence $u(t)$ [23, p. 287] may be considered for the modulation. Such a sequence with two states a and $-a$ and the minimum bit duration t_{bit} offers an autocorrelation of

$$\Psi_{uu}(\tau) = \begin{cases} a^2, & \text{if } \tau = k \cdot N_{\mathrm{seq}} \cdot t_{\mathrm{bit}}, k \in \mathbb{Z} \\ \frac{-a^2}{N_{\mathrm{seq}}}, & \text{otherwise} \end{cases} \tag{8}$$

for every shift of its length N_{seq}. The power spectrum of the sequence can be found with the Fourier transformation of $\Psi_{uu}(\tau)$ resulting in

$$S^2_{\mathrm{u}}(f) = \frac{a^2}{{N_{\mathrm{seq}}}^2}\delta(f) + a^2 \sum_{\substack{n=-\infty \\ n\neq 0}}^{\infty} \frac{N_{\mathrm{seq}}+1}{{N_{\mathrm{seq}}}^2}\,\mathrm{si}^2\left(\frac{n\cdot\pi}{N_{\mathrm{seq}}}\right)\delta\left(f-\frac{n}{t_{\mathrm{bit}}N_{\mathrm{seq}}}\right), \tag{9}$$

according to the Wiener–Khinchin theorem [24]. The resulting power spectrum of a modulation signal alternating between the "on" and "off" states can then be found by setting the amplitude of the binary sequence to $a = 0.5$ and adding a constant amplitude offset of 0.5 to the power spectrum of (9), resulting in

$$M^2(f) = \left(\frac{1}{4}+\frac{1}{4{N_{\mathrm{seq}}}^2}\right)\delta(f) + \frac{1}{4}\sum_{\substack{n=-\infty \\ n\neq 0}}^{\infty} \frac{N_{\mathrm{seq}}+1}{{N_{\mathrm{seq}}}^2}\,\mathrm{si}^2\left(\frac{n\cdot\pi}{N_{\mathrm{seq}}}\right)\delta\left(f-\frac{n}{t_{\mathrm{bit}}N_{\mathrm{seq}}}\right) \tag{10}$$

as the modulation power spectrum $M^2(f)$ of the pseudo-random sequence, as shown in Fig. 10. Considering long sequences with $N_{\mathrm{seq}} \gg 1$, the magnitudes of the spurious components are scaled approximately by $\frac{1}{N_{\mathrm{seq}}}$, while the constant component is unaffected. The distance $\frac{1}{N_{\mathrm{seq}}t_{\mathrm{bit}}}$ between the spurious components also decreases when N_{seq} is increased, resulting in a more closely populated spectrum of downscaled components instead of separated components that stand out. Therefore, a high N_{seq} should be implemented to reduce the appearance of spurious components. Even a moderate sequence length N_{seq} of 1024 increases the SFDR to over 30 dB for the example with a fixed 50% duty cycle. Ultimately, the maximum effective length of N_{seq} is limited by the observation time of the radar. Considering the appearance of spectral components created by the modulation, two possible mitigation strategies can be derived. First, when no randomization is implemented, the switching frequency can be selected high enough so that the spurious components fall outside the radar bandwidth. If this is not possible, randomization can be used to decrease the magnitude of undesired spectral components. This is revisited in the radar-specific section.

IV. SIMULATION RESULTS AND DISTORTIONS IN FMCW RADAR SYSTEMS

FMCW-based radar sensors are well established in the automotive sector due to the possibility of a relatively easy and low-cost implementation [25]. The operation principle is based on a continuous variation of the momentary transmit signal frequency $f_{\mathrm{m}}(t)$ with

$$f_{\mathrm{m}}(t) = f_{\mathrm{i}} \pm \mu \cdot t\,, \tag{11}$$

where f_{i} is the initial frequency and μ the chirp rate. As the frequency changes in a linear fashion over time, the reflected and transmitted signals differ in frequency relative to the round trip time. Fig. 11 shows a typical block diagram

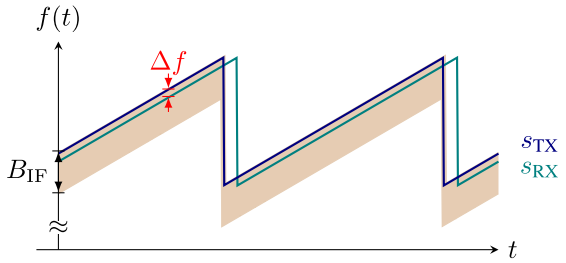

FIGURE 12. Representation of the FMCW signals over time. The difference in frequency between the sent and received signals allows the evaluation of the target distance. The combination of frequency downconversion and subsequent filtering can be represented as a bandpass filter that is shifted by the frequency of the transmit signal.

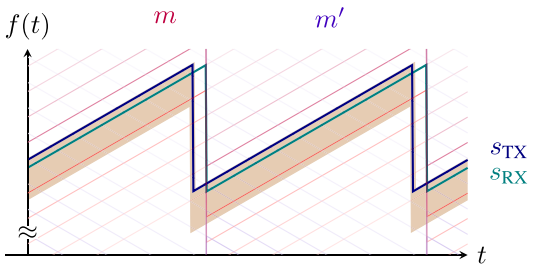

FIGURE 13. Representation of the FMCW signals over time for a modulated return signal. Additional signal components are present due to the modulation and may be interpreted as targets. Components that remain within the filter bandwidth are of particular concern.

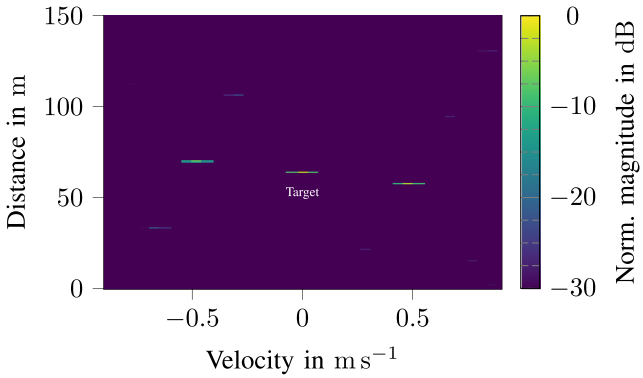

FIGURE 14. Simulation of modulated radar transponse. The simulated target is placed at the center at a distance of 65 m. The modulation frequency was set such that spurious components are clearly visible.

for FMCW radar. A signal that changes its frequency over time is generated and transmitted with an antenna. After the signal is reflected at a target, it is received by a second antenna. The currently generated signal is compared with the received signal with a mixer, which results in a beat signal at a relatively low frequency. The distance to a target can be obtained by evaluating the frequency of the beat signal. For a static target and a linear frequency change, the observed frequency is directly proportional to the distance to the target. Evaluation is usually done in the digital domain, for which an ADC is used with an anti-aliasing filter. The combination of the filter and the mixer can also be considered as tunable bandpass with a small bandwidth B_{IF} attached to the frequency of the transmitted signal $s_{\mathrm{tx}}(t)$. This will be beneficial for further evaluation of the behavior. The momentary frequencies of the transmitted and received signals over time are depicted in Fig. 12 for a single stationary target. As can be observed, the difference in frequency between the two signals remains constant for the larger part of the ramp. The evaluated bandwidth of the received radar signal depends on the combination of the frequency downconversion and the filtering before the ADC. As shown in Fig. 12, the evaluated frequency region shifts over time with the transmit signal. If the received signal experiences modulation, additional frequency components will be present, as the signal becomes convoluted with $M(f)$ according to (6). Graphically, this can be achieved by combining Figs. 12 and 9. Due to the signal distribution, as shown in Fig. 9, spurious components envelop the instantaneous frequency of $s_{\mathrm{rx}}(t)$. As $s_{\mathrm{rx}}(t)$ shifts in frequency, the dependent components are also shifted. The results are shown in Fig. 13. Additional frequency components m surround the initial unmodulated signal with equidistant spacing. Note that the negative component of $S_{\mathrm{rx}}(f)$ yields additional signal elements m' that appear as if mirrored on the time axis. However, this is only academic and has little relevance for practical considerations. First, these components are of negligible magnitude due to the dependence on the si-function. Additionally, the frequency change is of the incorrect sign, and therefore not correlated to a possible target. Although this might increase the noise floor in theory, unwanted ghost targets are not a concern. These considerations provide guidelines for practical implementations. First, signal components within the filter bandwidth should be avoided, if possible, to suppress the appearance of unwanted targets. For FMCW, this can be achieved relatively simply by selecting a short modulation period, which fulfills $T < \frac{1}{B_{\mathrm{IF}}}$. Alternatively, a randomization of the modulation signal $m(t)$ can be used. Changing $m(t)$ in such a way that the mean value of $s_{\mathrm{rx}}(t)$ is unaffected would result in the spreading of unwanted components, while the center frequency does not change. This will result in the reduced appearance of unwanted ghost targets due to the inherent processing gain achieved by the temporal integration of the FMCW radar. This examination suggests that the presented procedure offers good applicability for FMCW. For the sake of completeness, it must be noted that modern radar signal processing is based on multiple fast chirps that are combined to evaluate a scene. However, this does not change the previous considerations but beneficially increases the processing gain. To evaluate the behavior of FMCW, a simulated transpose was processed, as shown in Fig. 14. A simple PWM modulation with a duty cycle of 50% was chosen. The frequency of 755 kHz was selected similar to the one later used to create Fig. 17(b). The spurious components can be clearly observed with a high magnitude as predicted. Changing the modulation frequency can be used to move the appearance of the ghost targets. For switching frequencies outside the bandwidth B_{IF}, these unwanted ghost targets disappear as predicted.

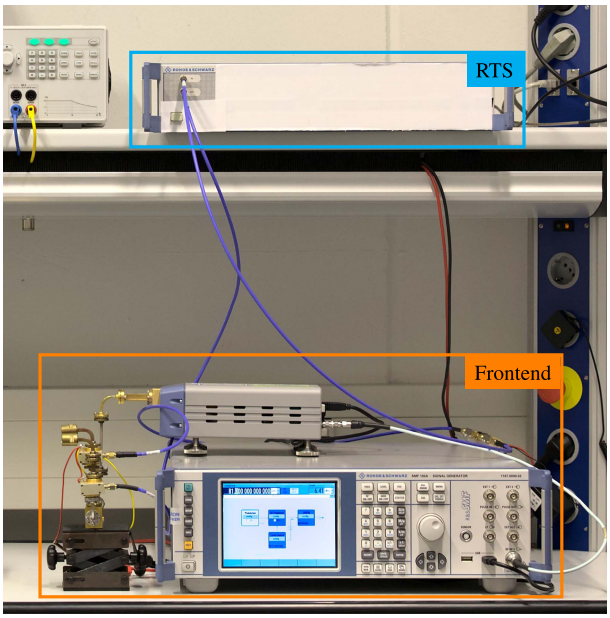

FIGURE 15. Test setup for evaluating the radar response. The field programmable gate array (FPGA)-based RTS is placed on the top. The up- and downconversion within the frontend is performed with two mixers fed by a signal source.

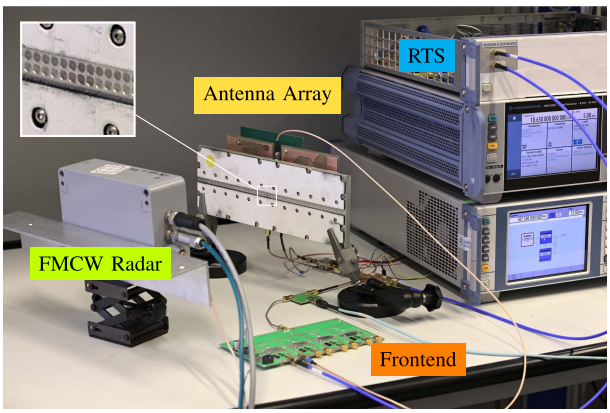

FIGURE 16. Test setup for the evaluating point target simulation with multiple angles. An antenna array is placed in front of an FMCW radar. Different elements of the antenna array are switched to a single target simulator backend to create multiple targets with differing angle.

V. MEASUREMENT RESULTS

A. TEST SETUP FOR DYNAMIC RANGE EVALUATION

To verify the claims made above and evaluate the characteristics in a real scenario, an existing digital RTS [6] is extended in accordance with the presented method. This allows the evaluation of the effects that switching has on the target evaluation. This implementation is based on predefined sequences, and the switching of the signal chain is applied by AND gates on a digital data stream, as shown in Fig. 5. For comparison, PWM and pulse density modulation (PDM) capabilities are implemented. While a perceived attenuation of the signal can be achieved with both, the PWM is based on equally spaced enable pulses, where the duration of the pulses is also the same for a desired attenuation value. The pulse density modulation (PDM), however, is implemented with randomization in such a way that the moving average of the "on" duration remains the same. A random sequence is generated beforehand by filling a string of zeros with a series of ones, where the ratio is determined by the desired attenuation value. The sequence is then randomly shuffled with the Python `random.shuffle()` implementation, which is based on the Mersenne-Twister pseudo-random number generator [26]. For this work, precalculated sequences are used; however, it would be possible to calculate the sequence directly on the field programmable gate array (FPGA) as very efficient and parallel implementations of pseudo-random number generators are possible [27]. The setup is shown in Fig. 15. The signal manipulation happens in the RTS, while the up- and downconversion is done with a mixing stage on the right side of the frontend followed by two horn antennas. An R&S SMF100 A signal source in combination with an SMZ90 frequency multiplier provides the local oscillator frequency for the conversion. For the examination, the commercial radar INRAS RADARBOOK is used. The parameters of the radar setup are noted in Table 1.

TABLE 1. System Parameters of the RUT

Symbol	Quantity	Value used
f_{i}	Carrier frequency	76.2 GHz
B_{RF}	RF bandwidth	600 MHz
T_{ch}	Chirp duration	512 µs
N_{chirp}	Number of chirps per sequence	64

B. EVALUATION OF DYNAMIC RANGE IMPROVEMENT AND GENERAL BEHAVIOR

The setup shown in Fig. 15 was used, and several sequences were tested with FMCW radar signals. Fig. 17 shows illustrative measurements in the range-Doppler domain for FMCW. All magnitudes are normalized for better visibility of the maximum component. Fig. 17(a) shows a constant target as a reference with no modulation applied. Unwanted ghost targets can be present with simple PWM-based modulation. The frequency used to generate Fig. 17(b) was set to 732 kHz; no ghost targets were observed at higher switching frequencies for the parameter set used. However, the unwanted ghost target created by the low switching frequency yields nearly the same magnitude as the desired target. No undesired effects could be observed for the PDM modulation. Fig. 18 shows a comparison of different PDM modulations. This modulation scheme allows variations of more than 30 dB without negative side effects observed in the experimental setup.

C. TEST SETUP FOR MULTIANGLE SCENARIOS

To evaluate the multiangle setup, a linear antenna array is combined with an RTS so that the backend can be switched

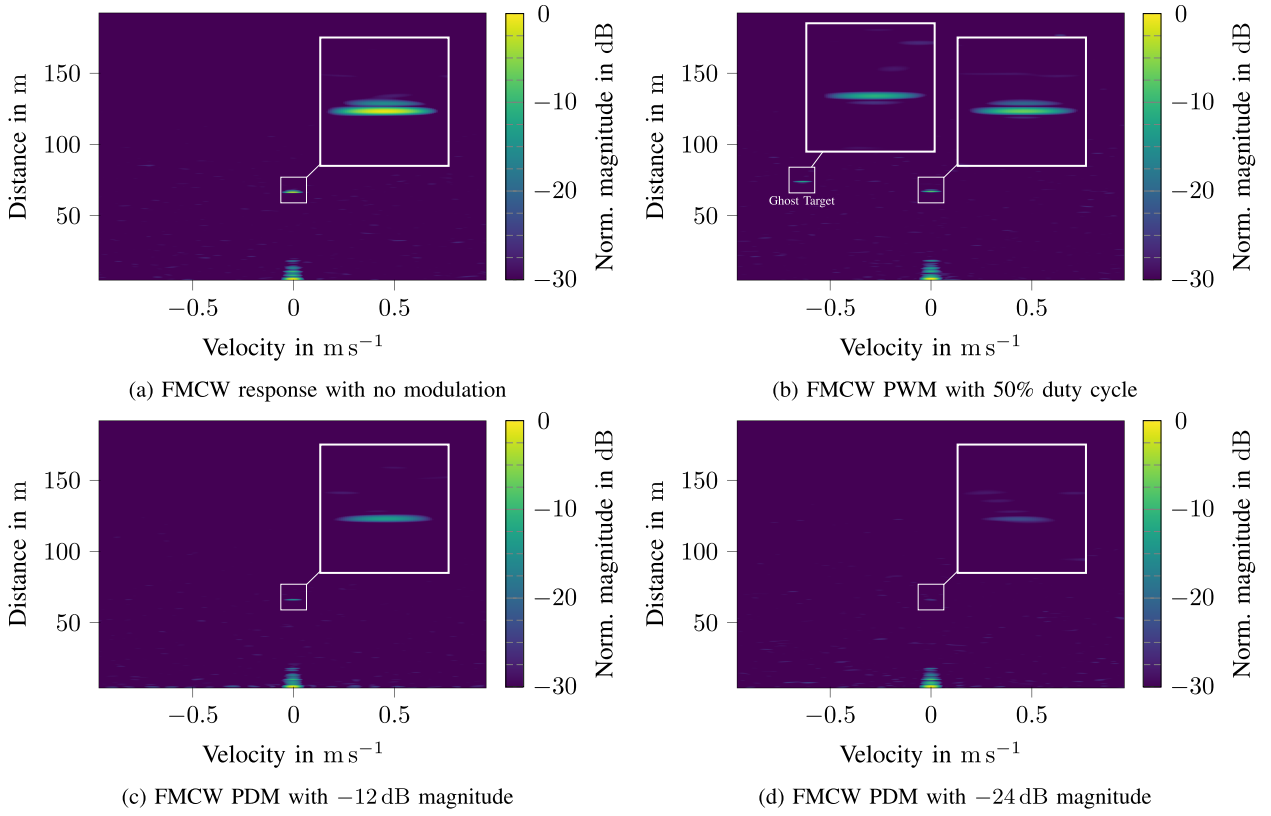

(a) FMCW response with no modulation

(b) FMCW PWM with 50% duty cycle

(c) FMCW PDM with −12 dB magnitude

(d) FMCW PDM with −24 dB magnitude

FIGURE 17. Measurement results of various target simulation settings. No modulation is used in the first image, while different modulations are applied for the other cases. All results are normalized for better comparability to the maximum magnitude within the data. Although the PDM settings used are the same, the PWM frequency differs to show the undesired effects created by the modulation.

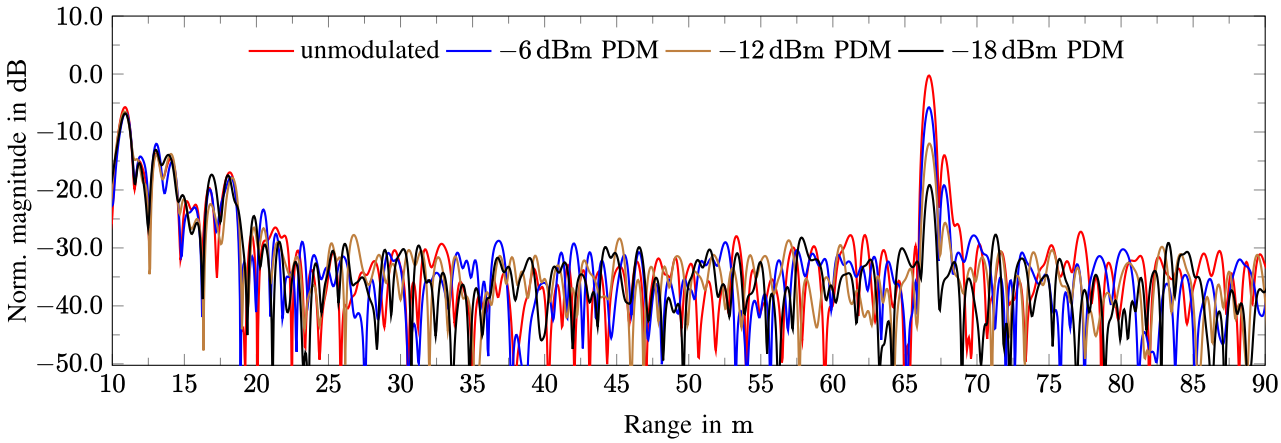

FIGURE 18. Comparison of varying magnitudes of the target power which are created by the PDM modulation. The level adjustment matches the set value with no observable deterioration compared to the unmodulated scenario.

between its individual elements, as shown in Fig. 16. The antenna array includes an X4 frequency multiplier for the transmit path and the received signal is divided by the same factor, increasing the usable bandwidth of the RTS backend [28]. In addition, the frontend consists of image reject mixers and an R&S SMA100B signal source. An R&S SMF100 A signal source is used as a reference for the RTS backend.

D. EVALUATION OF MULTIANGLE SCENARIO SIMULATIONS

The antenna array shown in Fig. 16 is taken from an R&S QAT100 and allows the selection of 96 element pairs to be used as a receive and transmit antennas. For the evaluation of two targets, the output and receive paths are alternated between two pairs. The processed radar image shown in Fig. 19 was generated using the 10th and 70th element combinations of the array. Each combination was enabled for 171.4 μs

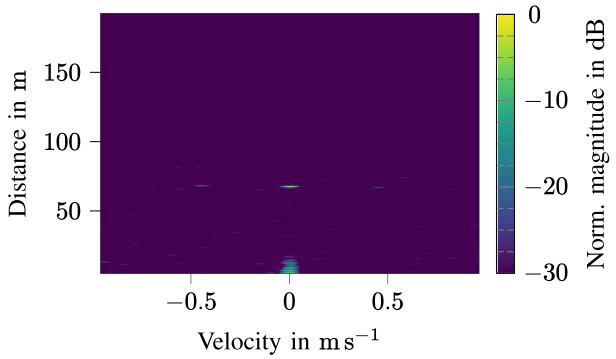

(a) Range-Doppler response

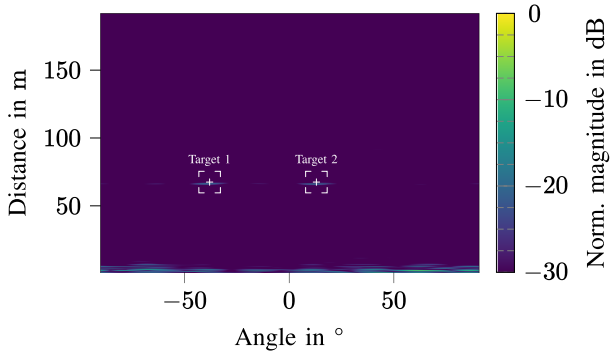

(b) Range-angle response

FIGURE 19. **Measurement of two simulated targets at the same distance varying in angle. There are noticeable ghost targets present due to the limited switching frequency of the antenna array.**

before switching to the other elements. The relatively low switching frequency of around 3 kHz is used due to the hardware limitations of the experimental setup. This results in multiple ghost targets, which can be observed in Fig. 19. However, two distinguishable targets are clearly present at the set positions.

VI. CONCLUSION

A. SUMMARY OF THE FINDINGS

The concept of an intermittent signal response to a radar sensor was investigated, and the practical advantages were discussed. It was shown that a great improvement in the dynamic range and considerable cost savings for future RTS are possible through relatively simple means. The theoretical implications of an additional modulation were examined and practical implementations used to prove real-world implications of the presented concept. The measured results for the experimental implementations show that an RTS for complex scenarios is feasible, with a single backend and moderate switching frequencies for FMCW RUTs. The test results show that a factor of around 1000 in signal strength is feasible, which may be used for dynamic range improvement or for the representation of a multitude of similar targets with different angles.

B. APPLICABILITY TO SENSORS BASED ON ADVANCED MODULATION

This work focuses on FMCW-based sensors, which make up the majority of radar systems used in the automotive sector. However, it should be noted that there are advanced concepts that warrant special consideration. For example, a switching process can be incorporated to achieve isolation between the transmit and receive paths when using a single antenna [29], [30], [31], or enable channel separation in multiple input multiple output (MIMO) concepts [32]. As a result, spurious components may already be present in the radar signal received by the RTS. This results in a multitude of spurious components according to Section III and the introduction of spurious components into the relevant bandwidth for practical switching frequencies. However, the randomization technique discussed earlier can be used to reduce the occurrence of unwanted ghost targets in this case. Another relevant development is given by the introduction of multifrequency radar signals [33] such as orthogonal frequency-division multiplexing (OFDM) [34]. Here, the available bandwidth is divided into equally spaced sections that are utilized by orthogonally spaced subcarriers. This also creates the problem of introducing spurious components into the relevant radar bandwidth. Randomization appears to be a promising means of reducing the occurrence of unwanted targets in this scenario as well. However, further research is required to make a more accurate statement regarding the limitations of this approach with advanced radar waveforms.

ACKNOWLEDGMENT

We would like to thank Steffen Neidhardt, Maximilian Bogner, Benedikt Simper, and Marius Brinkmann at Rohde & Schwarz for their insight and expertise. We acknowledge financial support by Deutsche Forschungsgemeinschaft and Friedrich-Alexander-Universität Erlangen-Nürnberg within the funding programme “Open Access Publication Funding”.

REFERENCES

[1] M. Steins, S. Müller, and A. R. Diewald, “Digital Doppler effect generation with CORDIC algorithm for radar target simulations,” in *Proc. 23rd Int. Conf. Appl. Electromagn. Commun.*, 2019, pp. 1–5.
[2] S. Wald, T. Mathy, S. Nair, C. M. Leon, and T. Dallmann, “ATRIUM: Test environment for automotive radars,” in *Proc. IEEE MTT-S Int. Conf. Microw. Intell. Mobility*, 2020, pp. 1–4.
[3] J. Iberle, M. A. Mutschler, P. A. Scharf, and T. Walter, “A radar target simulator for generating micro-Doppler-signatures of vulnerable road users,” in *Proc. 16th Eur. Radar Conf.*, 2019, pp. 17–20.
[4] A. Gruber et al., “Highly scalable radar target simulator for autonomous driving test beds,” in *Proc. Eur. Radar Conf.*, 2017, pp. 147–150.
[5] A. Diewald et al., “Radar target simulation for vehicle-in-the-loop testing,” *Vehicles*, vol. 3, no. 2, pp. 257–271, Jun. 2021.
[6] G. Körner, M. Hoffmann, S. Neidhardt, M. Beer, C. Carlowitz, and M. Vossiek, “Multirate universal radar target simulator for an accurate moving target simulation,” *IEEE Trans. Microw. Theory Techn.*, vol. 69, no. 5, pp. 2730–2740, May 2021.
[7] F. Arzur, M. L. Roy, A. Pérennec, G. Tanné, and N. Bordais, “Hybrid architecture of a compact, low-cost and gain compensated delay line switchable from 1 m to 250 m for automotive radar target simulator,” in *Proc. Eur. Radar Conf.*, 2017, pp. 239–242.

[8] R. Abou-Jaoude, M. Grace, D. Geller, K. Noujeim, D. Bradley, and W. Oldfield, "Low cost 76 GHz radar target simulator and test system," in *Proc. 30th Eur. Microw. Conf.*, 2000, pp. 1–4.
[9] W. Scheiblhofer, R. Feger, A. Haderer, and A. Stelzer, "A low-cost multi-target simulator for FMCW radar system calibration and testing," in *Proc. 47th Eur. Microw. Conf.*, 2017, pp. 343–346.
[10] F. Rafieinia and K. Haghighi, "ASGARDI: A novel frequency-based automotive radar target simulator," in *Proc. IEEE MTT-S Int. Conf. Microw. Intell. Mobility*, 2020, pp. 1–4.
[11] P. Schoeder, B. Schweizer, A. Grathwohl, and C. Waldschmidt, "Multitarget simulator for automotive radar sensors with unknown chirp-sequence modulation," *IEEE Microw. Wireless Compon. Lett.*, vol. 31, no. 9, pp. 1086–1089, Sep. 2021.
[12] M. E. Asghar et al., "Radar target simulator and antenna positioner for real-time over-the-air stimulation of automotive radar systems," in *Proc. 17th Eur. Radar Conf.*, 2021, pp. 95–98.
[13] T. Dallmann, J.-K. Mende, and S. Wald, "ATRIUM: A radar target simulator for complex traffic scenarios," in *Proc. IEEE MTT-S Int. Conf. Microw. Intell. Mobility*, 2018, pp. 1–4.
[14] A. Diewald, B. Nuß, M. Pauli, and T. Zwick, "Arbitrary angle of arrival in radar target simulation," *IEEE Trans. Microw. Theory Techn.*, vol. 70, no. 1, pp. 513–520, Jan. 2022.
[15] V. Giannini et al., "A 192-virtual-receiver 77/79 GHz GMSK code-domain MIMO radar system-on-chip," in *Proc. IEEE Int. Solid-State Circuits Conf.*, 2019, pp. 164–166.
[16] M. Gottinger et al., "Coherent automotive radar networks: The next generation of radar-based imaging and mapping," *IEEE J. Microwaves*, vol. 1, no. 1, pp. 149–163, Jan. 2021.
[17] C. Zuo and H. Jiang, "A simulation method of target echo power," in *Proc. IEEE 4th Int. Conf. Signal Image Process.*, 2019, pp. 294–298.
[18] H. Milosiu et al., "A 3-W 868-MHz wake-up receiver with −83 dBm sensitivity and scalable data rate," in *Proc. ESSCIRC*, 2013, pp. 387–390.
[19] M. I. Skolnik, *Introduction to Radar Systems* (McGraw-Hill Electrical Engineering Series), 3rd ed. Boston, MA, USA: McGraw Hill, 2001.
[20] H. Friis, "A note on a simple transmission formula," *Proc. IRE*, vol. 34, no. 5, pp. 254–256, May 1946.
[21] I. Matsunami, R. Nakamura, and A. Kajiwara, "RCS measurements for vehicles and pedestrian at 26 and 79 GHz," in *Proc 6th Int. Conf. Signal Process. Commun. Syst.*, 2012, pp. 1–4.
[22] E. J. Kim, C.-H. Cho, W. Kim, C.-H. Lee, and J. Laskar, "Spurious noise reduction by modulating switching frequency in DC-to-DC converter for RF power amplifier," in *Proc. IEEE Radio Freq. Integr. Circuits Symp.*, 2010, pp. 43–46.
[23] P. L. Fernando, *Messtechnik*, 10th ed. Berlin, Heidelberg: Springer Vieweg, 2015.
[24] I. G. Cumming, "Autocorrelation function and spectrum of a filtered, pseudorandom binary sequence," *Proc. Inst. Elect. Eng.*, vol. 114, no. 9, pp. 1360–1362, Sep. 1967.
[25] J. Hasch, E. Topak, R. Schnabel, T. Zwick, R. Weigel, and C. Waldschmidt, "Millimeter-wave technology for automotive radar sensors in the 77 GHz frequency band," *IEEE Trans. Microw. Theory Techn.*, vol. 60, no. 3, pp. 845–860, Mar. 2012.
[26] M. Matsumoto and T. Nishimura, "Mersenne twister: A 623-dimensionally equidistributed uniform pseudo-random number generator," *ACM Trans. Model. Comput. Simul.*, vol. 8, no. 1, pp. 3–30, Jan. 1998.
[27] X. Tian and K. Benkrid, "Mersenne twister random number generation on FPGA CPU and GPU," in *Proc. NASA/ESA Conf. Adaptive Hardware Syst.*, 2009, pp. 460–464.
[28] G. Körner, C. Birkenhauer, P. Stief, C. Carlowitz, and M. Vossiek, "Efficient bandwidth enhanced multirate radar target simulation," in *Proc. IEEE/MTT-S Int. Microw. Symp.*, 2022, pp. 534–537.
[29] P. Almorox-Gonzalez, J.-T. Gonzalez-Partida, M. Burgos-Garcia, B. P. Dorta-Naranjo, and J. Gismero, "Millimeter-wave sensor with FMICW capabilities for medium-range high-resolution radars," *IEEE Trans. Microw. Theory Techn.*, vol. 57, no. 6, pp. 1479–1486, Jun. 2009.
[30] J. T. González-Partida, M. Burgos-García, B. P. Dorta-Naranjo, and F. Pérez-Martínez, "Stagger procedure to extend the frequency modulated interrupted continuous wave technique to high resolution radars," *IET Radar, Sonar Navigat.*, vol. 1, no. 4, pp. 281–288, Aug. 2007.
[31] J. A. McGregor, E. M. Poulter, and M. J. Smith, "Switching system for single antenna operation of an s-band FMCW radar," *Inst. Elect. Eng. Proc. Radar, Sonar Navigat.*, vol. 141, no. 4, pp. 241–248, Aug. 1994.
[32] R. Feger, C. Pfeffer, and A. Stelzer, "A frequency-division MIMO FMCW radar system based on delta," *IEEE Trans. Microw. Theory Techn.*, vol. 62, no. 12, pp. 3572–3581, Dec. 2014.
[33] N. Levanon, "Multifrequency radar signals," in *Proc. Rec. IEEE Int. Radar Conf.*, 2000, pp. 683–688.
[34] C. Sturm, T. Zwick, and W. Wiesbeck, "An OFDM system concept for joint radar and communications operations," in *Proc. VTC Spring - IEEE 69th Veh. Technol. Conf.*, 2009, pp. 1–5.

CHRISTOPH BIRKENHAUER (Graduate Student Member, IEEE) received the M.Sc. degree in electrical engineering from Friedrich-Alexander-Universität Erlangen-Nürnberg (FAU), Erlangen, Germany, in 2019, where he is currently working toward the Ph.D. degree. After graduation, he joined the Institute of Microwaves and Photonics (LHFT), FAU. His research interests include radar hardware design, radar target simulation, and system design.

GEORG KÖRNER received the B.Eng. degree in electrical engineering from TH Nürnberg Georg-Simon-Ohm, Nuremberg, Germany, in 2015, and the M.Sc. degree in information and communication technologies from Friedrich-Alexander-Universität Erlangen-Nürnberg (FAU), Erlangen, Germany, in 2017. From 2014 to 2016, he was a Research Assistant in the field of fiberoptic photonics with Siemens AG, Munich, Germany. After graduation, he joined the Institute of Microwaves and Photonics (LHFT), FAU, in 2017. His research interests include radar signal processing and radar hardware.

PATRICK STIEF received the B.Sc. and M.Sc. degrees in electrical engineering from Friedrich-Alexander-Universität Erlangen-Nürnberg (FAU), Erlangen, Germany, in 2016 and 2018, respectively, where he is currently working toward the Ph.D. degree. In 2019, he joined the Institute of Microwaves and Photonics (LHFT), FAU. His research interests include radar signal processing, radar target simulation, radar imaging, and machine learning-based radars.

GERHARD F. HAMBERGER received the B.Sc., M.Sc., and Dr.-Ing. degrees in electrical and computer engineering from the Technical University of Munich, Munich, Germany, in 2012, 2014, and 2019, respectively. In 2018, he joined the Systems and Projects Department of Rohde & Schwarz, Munich, Germany, where he worked on various state-of-the-art 5G test systems and electromagnetic field transformation software. In 2019, he became a Senior Development Expert with the Microwave Imaging Department of Rohde & Schwarz, Munich, Germany, focusing on automotive radar and radome test systems.

MATTHIAS BEER received the Dipl.Ing. degree in electrical engineering from the University of Applied Sciences Munich, Munich, Germany, in 2003, and the MBA degree in international management from the Munich University of Economics and Management, Munich, in 2012. From 2003 to 2007, he was an RF Design and Verification Engineer for Infineon Technologies, Munich, in the field of RF transceivers for 2G and 3G mobile communication devices. From 2007 to 2012, he was a Regional Application Manager of the Asia/Pacific region and a Product Manager with Rohde & Schwarz, Munich. From 2012 to 2014, he was setting up a European subsidiary for Focus Microwaves as a General Manager. Since 2014, he has been with Rohde & Schwarz GmbH & Co. KG as a Senior Expert in different positions. In his current position as the Director of hardware imaging sensors products, he is focusing on automotive radar and autonomous driving topics.

CHRISTIAN CARLOWITZ (Member, IEEE) received the Dipl.-Ing. degree in information technology from the Clausthal University of Technology, Clausthal-Zellerfeld, Germany, in 2010, and the Dr.-Ing. degree from the Friedrich-Alexander-Universität Erlangen-Nürnberg (FAU), Erlangen, Germany, in May 2018, for his thesis on wireless high-speed communication based on regenerative sampling. He is currently with the Institute of Microwaves and Photonics, FAU, where he has led the Microwave and Photonic Systems Group since 2018. His research interests include the conception, design, and implementation of innovative system architectures for radar and communication frontends at microwave, mm-wave, optical frequencies, hardware concepts, and analog and digital signal processing techniques, for ultra-wideband high-speed communication systems, full-duplex mobile communication transceivers, massive MIMO base stations, and for ranging and communication with mm-wave RFID systems. Dr. Carlowitz is a member of the IEEE Microwave Theory and Technology Society (MTT-S). He also is a Member of the IEEE MTT-S Technical Committee RF/Mixed-Signal Integrated Circuits and Signal Processing (MTT-15). He is a regular reviewer of IEEE TRANSACTIONS ON MICROWAVE THEORY AND TECHNIQUES. He is a member of the International Microwave Symposium (IMS) Technical Program Review Committee and a regular reviewer for several additional international conferences, including EuMW and ICMIM.

MARTIN VOSSIEK (Fellow, IEEE) received the Ph.D. degree from Ruhr-Universität Bochum, Bochum, Germany, in 1996. In 1996, he joined Siemens Corporate Technology, Munich, Germany, where he was the Head of the Microwave Systems Group from 2000 to 2003. Since 2003, he has been a Full Professor with Clausthal University, Clausthal-Zellerfeld, Germany. Since 2011, he has also been the Chair of the Institute of Microwaves and Photonics (LHFT), Friedrich-Alexander-Universität Erlangen-Nürnberg (FAU), Erlangen, Germany. He has authored or coauthored more than 300 articles. His research has led to more than 90 granted patents. His research interests include radar, transponder, RF identification, communication, and wireless locating systems. Dr. Vossiek is currently a member of the German National Academy of Science and Engineering (acatech) and the German Research Foundation (DFG) Review Board. He is also a member of the German IEEE Microwave Theory and Techniques (MTT)/Antennas and Propagation (AP) Chapter Executive Board and the IEEE MTT Technical Committees MTT-24 Microwave/mm-Wave Radar, Sensing, and Array Systems, MTT-27 Connected and Autonomous Systems (as the Founding Chair), and the MTT-29 Microwave Aerospace Systems. He also serves on the Advisory Board of the IEEE CRFID Technical Committee on Motion Capture & Localization. He is a member of organizing committee and technical program committee for many international conferences. He has served on review boards for numerous technical journals. He was the recipient of more than ten best paper prizes and several other awards. He was also the recipient of the 2019 Microwave Application Award from the IEEE MTT Society (MTT-S) for Pioneering Research in Wireless Local Positioning Systems. From 2013 to 2019, he was an Associate Editor of IEEE TRANSACTIONS ON MICROWAVE THEORY AND TECHNIQUES.